

DFR: DEPTH FROM ROTATION BY UNCALIBRATED IMAGE RECTIFICATION WITH LATITUDINAL MOTION ASSUMPTION

Yongcong Zhang^{1,*} Yifei Xue^{2,*} Ming Liao² Huiqing Zhang¹ Yizhen Lao^{1,†}

¹ Hunan University

² Jiangxi Provincial Natural Resources Cause Development Center

Abstract—Despite the increasing prevalence of rotating-style capture (e.g., surveillance cameras), conventional stereo rectification techniques frequently fail due to the rotation-dominant motion and small baseline between views. In this paper, we tackle the challenge of performing stereo rectification for uncalibrated rotating cameras. To that end, we propose Depth-from-Rotation (DfR), a novel image rectification solution that analytically rectifies two images with two-point correspondences and serves for further depth estimation. Specifically, we model the motion of a rotating camera as the camera rotates on a sphere with fixed latitude. The camera’s optical axis lies perpendicular to the sphere’s surface. We call this latitudinal motion assumption. Then we derive a 2-point analytical solver from directly computing the rectified transformations on the two images. We also present a self-adaptive strategy to reduce the geometric distortion after rectification. Extensive synthetic and real data experiments demonstrate that the proposed method outperforms existing works in effectiveness and efficiency by a significant margin.

Index Terms—Structure-from-Motion, stereo rectification, image matching

I. INTRODUCTION

Image rectification is vital for efficient stereo matching by forcing the point correspondence restricted in the same scan line (row). This process significantly reduces the computational cost for further depth estimation and thus is widely used in 3D vision applications, such as robotics, autonomous driving, and augmented reality.

Motivations. Classical image rectification techniques apply homographies on a pair of images (i.e., the master and the slave image) whose epipolar geometry is pre-computed. Thus the epipolar lines in the original images map to horizontally aligned lines in the transformed images [1].

However, we found the ubiquitous 2D rotating cameras, such as surveillance cameras and tripod head cameras on UAVs (Fig. 2), fail in applying conventional image rectifica-

This work is supported by the National Key R&D Program of China (No. 2022ZD0119003), Nature Science Foundation of China (No. 62102145), and Jiangxi Provincial 03 Special Foundation and 5G Program (Grant No. 20224ABC03A05).

*Both authors contributed equally to this research.

†Corresponding author: yizhenlao@hnu.edu.cn.

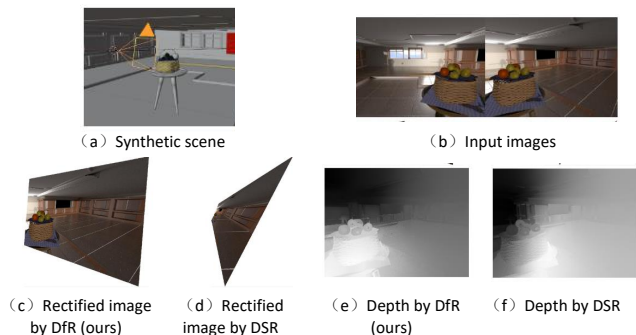


Fig. 1: A rotating camera (a) captures two images (b). Stereo rectified results and estimated depth map by proposed method *DfR* (c)(e) and state-of-the-art work *DSR* [6] (d)(f).

tion for the three shortcomings shared in the existing works (Fig. 1):

1) Cumbersome calibration. The works of [2], [3] require off-line intrinsic calibration and have to fix the camera setting, such as focal length. However, such cumbersome and stringent requirements are challenging to maintain in real-world applications.

2) Poor epipolar geometry estimation with short baseline. Another type of rectification methods [4], [5] demand estimated epipolar geometry as input. Note that accurate epipolar computation is highly dependent on establishing a sufficient baseline between images so that the rectification can be reliably estimated. However, the rotating cameras produce extremely short baselines that violate such an assumption.

3) Over-distorted rectification. Existing solutions could lead to significant geometric distortion among rectified images once the slave and master images have significant relative rotation, which is not preferred for high-quality depth-based applications [6].

Contributions. This paper tackles the challenge of stereo rectification for uncalibrated rotating cameras with extremely short baselines. To this end, we propose a novel image rectification solution that analytically computes the rectified

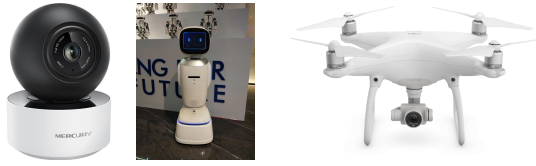


Fig. 2: Typical rotating camera systems.

transformations to the two images with only two-point correspondences and serves for the further depth estimation, short for Depth-from-Rotation (**DFR**). Specifically, we model the motion of a rotating camera as the camera rotates on a sphere with fixed latitude. The camera’s optical axis lies perpendicular to the sphere’s surface. We call this **”latitudinal motion assumption”**. Then we derive a 2-point analytical solver that computes the rectified transformations for the two images directly. We also present a self-adaptive strategy to reduce the geometric distortion after rectification.

Previous research [3] presents structure from motion (SfM) solution with spherical motion, which is similar to our latitudinal motion. However, we want to highlight that [3] requires accurate pre-calibration of intrinsic while the proposed **DFR** is a calibration-free method. Besides, the radius of sphere in [3] is assumed as brachium ($\approx 0.8m$) while with only a centimeter length for rotating camera case. The most related work [6] rectifies uncalibrated cameras with slight movements. Nevertheless, such a method assumes a small but pure translation by neglecting the rotation. In contrast, we consider both rotation and translation produced by latitudinal motion.

Differing from previous methods, our contributions are:

- We describe the rotating camera as a latitudinal motion and find that rectified transformations for such a case can be computed directly and efficiently with only two-point correspondences.
- Extensive experiments demonstrate that the proposed rectification method **DFR** outperforms state-of-the-art techniques in align accuracy and distortion suppression. The code has been uploaded to GitHub¹.

II. RELATED WORK

Finding the epipolar geometry is the critical step in the previous approach to launching the rectification. A detailed review of the related techniques is in [7]. Typically, [4] proposes to compute the fundamental matrix first and then extract the homographies followed by a decomposing to reduce the geometric distortion. Gluckman and Nayar [8] present a rectification approach that minimizes the re-sampling effect. [9] introduces an implicit image rectification approach by computing homographies directly from point correspondences. [10] alternatively utilizes a Quasi-Euclidean-based rectification algorithm. More recently, [6] proposes a direct uncalibrated image rectification solution for the monocular camera with a small translation.

¹<https://github.com/zhangtaxue/DFR>

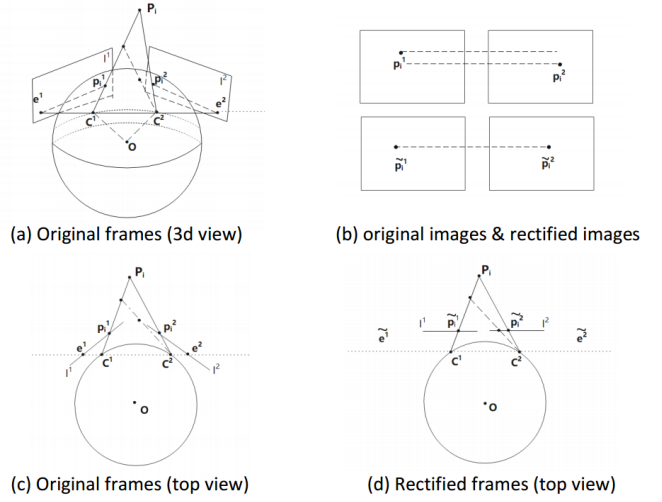


Fig. 3: 3D view of general latitudinal motion (a). The objective of our rectification is to shift the original frames (c) to the rectified frames (d), this process also map the original images to the rectified ones (b).

As opposed to existing methods that require calibrated stereo rig, estimated epipolar geometry, or pure translation assumption, we propose a practical solution called DfR to rectify two uncalibrated images captured by a rotating camera with an extremely short baseline.

III. METHODOLOGY

A. The Geometry of Latitudinal Camera Motion

We highlight that the rotating camera, such as a surveillance camera, follows a **”latitudinal camera motion”** trajectory. With this assumption, the camera rotates at a constant latitude C^1C^2 with a fixed distance from an origin, and the optical axis is aligned with the ray between the origin and camera center $\overrightarrow{OC^1}$ (Fig. 3(a)(c)).

Assuming a 3D point $\mathbf{P}_i = [X_i, Y_i, Z_i]^\top$ is captured by C^1 and C^2 as $\mathbf{p}_i^1 = [x_i^1, y_i^1]$ and $\mathbf{p}_i^2 = [x_i^2, y_i^2]$:

$$\alpha_i[\mathbf{p}_i^j, 1]^\top = \mathbf{K}^j[\mathbf{R}^j|\mathbf{t}^j][\mathbf{P}_i, 1]^\top \quad (1)$$

where $\mathbf{R}^j \in SO(3)$ and $\mathbf{t}^j \in \mathbb{R}^3$ are rotation matrix and translation vector of j^{th} camera. α_i is a scalar w.r.t depth. \mathbf{K} is a 3×3 matrix known as the calibration matrix containing the intrinsic parameters of a camera. Since the majority of the existing works assume the principal points are usually also close to the image center and \mathbf{K} keeps constant between two views [1], we adhere to this assumption too in this paper. Thus $\mathbf{K} = \mathbf{K}^1 = \mathbf{K}^2$ are defined as:

$$\mathbf{K} = \text{diag}(f_x, f_y, 1) \quad (2)$$

where f_x and f_y are focal lengths along x and y axes.

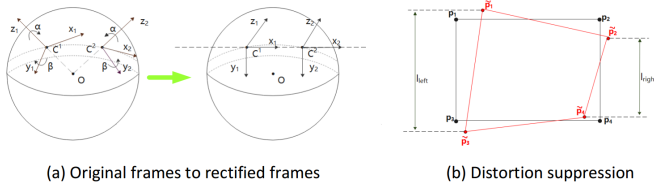


Fig. 4: (a) The transformation of camera coordinate system between original and rectified frames. (b) Geometric distortion suppression.

B. Finding the Rectified Matrices

The primary aim of the rectification that we seek is to transform the stereo under latitudinal camera motion into a laterally displaced stereo setting (fig. 3(d)). We present a novel rectification solution which leads to such transformation.

Specifically, we derive the rotation-based rectification (Sect. III-B1) and introduce the analytical solver for rectified matrices (Sect. III-B2). We also present a self-adaptive strategy to suppress the geometric distortion (Sect. III-B3) and integrate these steps into a complete rectification pipeline (Sect. III-C).

1) Derivation of Rectified Matrices to C^1 and C^2 :

We show that stereo $C^1 \leftrightarrow C^2$ under latitudinal camera motion can be rectified to laterally displaced stereo $\tilde{C}^1 \leftrightarrow \tilde{C}^2$ by applying two homographies \mathbf{H}_1 and \mathbf{H}_2 to C^1 and C^2 respectively.

Proposition 1. When two views C^1 and C^2 have a constant but unknown focal length and under latitudinal camera motion, after applying the \mathbf{H}_1 and \mathbf{H}_2 defined as

$$\mathbf{H}^1 = \begin{bmatrix} \cos(\beta)\cos(\alpha) & -\frac{f_x \sin(\alpha)\sin(b)}{f_y} & -f_x \cos(\alpha)\sin(\beta) \\ \frac{f_y \cos(\beta)\sin(\alpha)}{f_x} & \cos(\alpha) & -f_y \sin(\alpha)\sin(\beta) \\ \frac{\sin(\beta)}{f_x} & 0 & \cos(\beta) \end{bmatrix} \quad (3)$$

$$\mathbf{H}^2 = \begin{bmatrix} \cos(\beta)\cos(\alpha) & \frac{f_x \sin(\alpha)\sin(b)}{f_y} & f_x \cos(\alpha)\sin(\beta) \\ -\frac{f_y \cos(\beta)\sin(\alpha)}{f_x} & \cos(\alpha) & -f_y \sin(\alpha)\sin(\beta) \\ -\frac{\sin(\beta)}{f_x} & 0 & \cos(\beta) \end{bmatrix} \quad (4)$$

to C^1 and C^2 respectively, they will be transform to \tilde{C}^1 and \tilde{C}^2 that under perfect laterally displace. Where α and β are two angles that control the rotations of C^1 and C^2 .

Proof. As shown in Fig. 4(a), we assume the frames of C^1 and C^2 are w.r.t world coordinate system O . Thus, with latitudinal camera motion assumption, the poses of C^1 and C^2 are:

$$[\mathbf{R}^1 | \mathbf{t}^1] = [R(\alpha, -\beta, 0), \mathbf{z}] \quad (5)$$

$$[\mathbf{R}^2 | \mathbf{t}^2] = [R(-\alpha, \beta, 0), \mathbf{z}] \quad (6)$$

where $\mathbf{z} = [0, 0, -1]^\top$ and $R(\alpha, \beta, \gamma) = R_z(\alpha)R_y(\beta)R_x(\gamma)$ is the matrix multiplication of atomic matrices whose yaw, pitch, and roll angles are α, β, γ . Thus, \mathbf{R}^1 and \mathbf{R}^2 are:

$$\mathbf{R}^1 = \begin{bmatrix} \cos(\beta)\cos(\alpha) & \sin(\alpha) & \cos(\alpha)\sin(\beta) \\ -\cos(\beta)\sin(\alpha) & \cos(\alpha) & -\sin(\beta)\sin(\alpha) \\ -\sin(\beta) & 0 & \cos(\alpha) \end{bmatrix} \quad (7)$$

$$\mathbf{R}^2 = \begin{bmatrix} \cos(\beta)\cos(\alpha) & -\sin(\alpha) & -\cos(\alpha)\sin(\beta) \\ \cos(\beta)\sin(\alpha) & \cos(\alpha) & -\sin(\beta)\sin(\alpha) \\ \sin(\beta) & 0 & \cos(\alpha) \end{bmatrix} \quad (8)$$

Obviously, we can rotate C^1 and C^2 to coincide with the world frame by rotation matrices $\mathbf{R}^{1^{-1}}$ and $\mathbf{R}^{2^{-1}}$. Note that with such a setting, the two novel views are laterally displaced stereo. Thus, the homographies which can perform the rectification are:

$$\mathbf{H}^1 = \mathbf{K}\mathbf{R}^{1^{-1}}\mathbf{K}^{-1} \quad \mathbf{H}^2 = \mathbf{K}\mathbf{R}^{2^{-1}}\mathbf{K}^{-1} \quad (9)$$

Finally, by subsisting Eq. (7), Eq. (8) and Eq. (9), we can obtain Eq. (3) and Eq. (4). \square

2) Computation of \mathbf{H}^1 and \mathbf{H}^2 :

• **Decomposition of \mathbf{H}^1 and \mathbf{H}^2 .** Follows the homograph decomposition introduced in [4], we express the rectified homographies in Proposition 1 as the matrix multiplication of two 3×3 matrices:

$$\mathbf{H}^1 = \mathbf{H}_s^1 \mathbf{H}_y^1 \quad \mathbf{H}^2 = \mathbf{H}_s^2 \mathbf{H}_y^2 \quad (10)$$

where,

$$\mathbf{H}_s^1 = \begin{bmatrix} S_a & S_b & 0 \\ 0 & 1 & 0 \\ 0 & 0 & 1 \end{bmatrix} \quad \mathbf{H}_s^2 = \begin{bmatrix} S_a & -S_b & 0 \\ 0 & 1 & 0 \\ 0 & 0 & 1 \end{bmatrix} \quad (11)$$

$$\mathbf{H}_y^1 = \begin{bmatrix} 1 & 0 & 0 \\ h_{21} & h_{22} & h_{23} \\ h_{31} & 0 & h_{33} \end{bmatrix} \quad \mathbf{H}_y^2 = \begin{bmatrix} 1 & 0 & 0 \\ -h_{21} & h_{22} & h_{23} \\ -h_{31} & 0 & h_{33} \end{bmatrix} \quad (12)$$

We use \mathbf{H}_y^1 and \mathbf{H}_y^2 to align the correspondences along the y-axis while \mathbf{H}_s^1 and \mathbf{H}_s^2 serve to reduce the geometric distortion of the transformed images.

• **Computation of \mathbf{H}_y^1 and \mathbf{H}_y^2 .** Notice that the elements of \mathbf{H}_y^1 and \mathbf{H}_y^2 share the same values $h_{21}, h_{22}, h_{23}, h_{31}$, and h_{33} but with different signs. Thus, we can compute \mathbf{H}_y^1 and \mathbf{H}_y^2 by recovering the values of these elements.

Proposition 2. Given two-point correspondences $\mathbf{p}_1^1 \leftrightarrow \mathbf{p}_1^2$ and $\mathbf{p}_2^1 \leftrightarrow \mathbf{p}_2^2$, we first arbitrarily set the values of h_{22} and h_{23} and then obtain

$$h_{31} = \frac{t_1}{h_{22}}, \quad h_{33} = \frac{1}{h_{22}}, \quad h_{21} = t_1 h_{23} + t_2 h_{22} \quad (13)$$

where t_1 and t_2 can be extracted by $\mathbf{t} = \mathbf{A}^{-1}\mathbf{b}$ with following definition:

$$\underbrace{\begin{bmatrix} -(x_1^2 y_1^1 + x_1^1 y_1^2) & (x_1^1 + x_1^2) \\ -(x_2^2 y_2^1 + x_2^1 y_2^2) & (x_2^1 + x_2^2) \end{bmatrix}}_{\mathbf{A}} \underbrace{\begin{bmatrix} t_1 \\ t_2 \end{bmatrix}}_{\mathbf{T}} = \underbrace{\begin{bmatrix} -y_1^1 + y_1^2 \\ -y_2^1 + y_2^2 \end{bmatrix}}_{\mathbf{b}} \quad (14)$$

where \mathbf{A} and \mathbf{b} are 2×2 matrix and 2×1 vector consisted by the coordinates of the two correspondences.

Proof. By given a point correspondence $\mathbf{p}_i^1 \leftrightarrow \mathbf{p}_i^2$, we minimize the vertical alignment error after applying \mathbf{H}_y^1 and \mathbf{H}_y^2 via

$$[\mathbf{H}_y^1, \mathbf{H}_y^2] = \arg \min \sum_i \left(\frac{h_2^1 \mathbf{p}_i^1}{h_3^1 \mathbf{p}_i^1} - \frac{h_2^2 \mathbf{p}_i^2}{h_3^2 \mathbf{p}_i^2} \right)^2 \quad (15)$$

where \mathbf{h}_x^y is the x^{th} row of \mathbf{H}^y . Let

$$\frac{h_2^1 \mathbf{p}_i^1}{h_3^1 \mathbf{p}_i^1} - \frac{h_2^2 \mathbf{p}_i^2}{h_3^2 \mathbf{p}_i^2} = 0, \quad (16)$$

we can substitute elements of \mathbf{H} in Eq. (12) and coordinates of \mathbf{p}_i into Eq. (16)

$$h_{22} h_{31} (-x_i^2 y_i^1 - x_i^1 y_i^2) + (-h_{23} h_{31} + h_{21} h_{33}) (x_i^1 + x_i^2) = (y_i^2 - y_i^1) \quad (17)$$

where we force $h_{22} h_{33} = 1$ since homography matrix is up to scale. Then with two-point correspondences $i = 1, 2$, we can get Eq. (14). \square

• **Computation of \mathbf{H}_s^1 and \mathbf{H}_s^2 .** We employ the method introduced in [4] to compute S_a and S_b . Since this section does not contain our contributions, we provide only the essential information for understanding the remainder of this paper. More details of the algorithm are available in [4], [6].

3) Geometric Distortion Suppression:

Recall that proposition 1 can hold with arbitrary value settings of h_{22} and h_{23} . However, we point out that their values decide the geometric distortion level. Thus, a good value choice of h_{22} and h_{23} suppresses the distortion after rectification.

Experimentally, we found out that the value of h_{23} has a tiny inference about the shape of the output frame. Thus, it is critical to decide the value of h_{22} . As shown in Fig. 4(b), we assume the vertexes of original frame are $\mathbf{p}_1 = [-\frac{W}{2}, -\frac{H}{2}, 1]^T$, $\mathbf{p}_2 = [\frac{W}{2}, -\frac{H}{2}, 1]^T$, $\mathbf{p}_3 = [-\frac{W}{2}, \frac{H}{2}, 1]^T$, and $\mathbf{p}_4 = [\frac{W}{2}, \frac{H}{2}, 1]^T$ (H and W are the height and width of image). After rectification by applying \mathbf{H}^1 and \mathbf{H}^2 , the four vertexes becomes $\tilde{\mathbf{p}}_1, \tilde{\mathbf{p}}_2, \tilde{\mathbf{p}}_3$, and $\tilde{\mathbf{p}}_4$. Based on the description of \mathbf{H}^1 and \mathbf{H}^2 in Eq. (9), we can measure the heights of the left edge and right edge as

$$\begin{cases} l_{left} = \tilde{p}_3^y - \tilde{p}_1^y = \frac{2Hh_{22}^2}{2-t_1W} - H \\ l_{right} = \tilde{p}_4^y - \tilde{p}_2^y = \frac{2Hh_{22}^2}{2+t_1W} - H \end{cases} \quad (18)$$

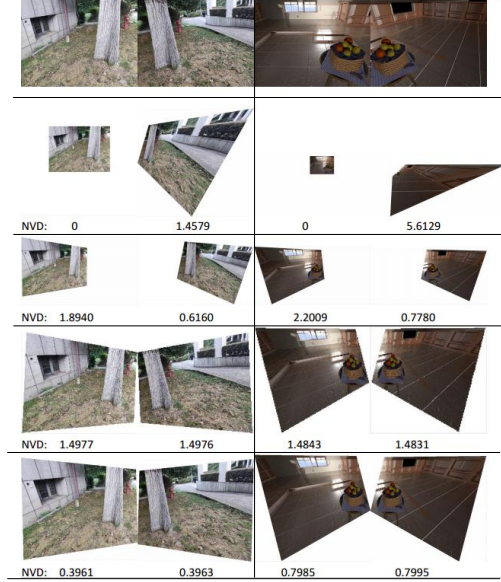


Fig. 5: Ablation study on the geometric distortion suppression. The input images (1st row) are rectified by *DSR* [6] (2nd row), *Loop* [4] (3rd row), proposed *DfR* with (5th row) and without self-adaptive distortion suppression module (4th row). The NVD scores are given below for each result.

To reduce the geometric distortion, we force $l_{left} + l_{right} = 2H$. Thus, we have the instruction to set h_{22} :

$$h_{22} = \sqrt{\frac{4-W^2t_1^2}{2}} \quad (19)$$

C. Pipeline

Note that we can only use two-point correspondences to perform rectification. However, we propose a RANSAC-like framework to robustly estimate the rectified matrices \mathbf{H}^1 and \mathbf{H}^2 by using the vertical alignment error **VAE** between y coordinates of a rectified correspondence $\tilde{\mathbf{p}}_l = [\tilde{x}_l \tilde{y}_l]^T$ and $\tilde{\mathbf{p}}_r = [\tilde{x}_r \tilde{y}_r]^T$

$$\text{VAE} = \frac{\sum_{i=1}^n (|\tilde{y}_{li} - \tilde{y}_{ri}|)}{n} \quad (20)$$

We describe the complete rectification pipeline in Alg. 1.

IV. EXPERIMENT

A. Synthetic Data

• **Comparison Methods.** We compare the proposed method *DfR* against to two state-of-the-art works:

- *Loop* [4]: Classical uncalibrated stereo rectification approach.
- *DSR* [6]: Direct stereo rectification with small motion assumption.
- *DfR*: The proposed method in this paper.

• **Metrics.** We evaluate the solutions by two metrics:

- **VAE**: Vertical alignment error defined in Eq. (20).

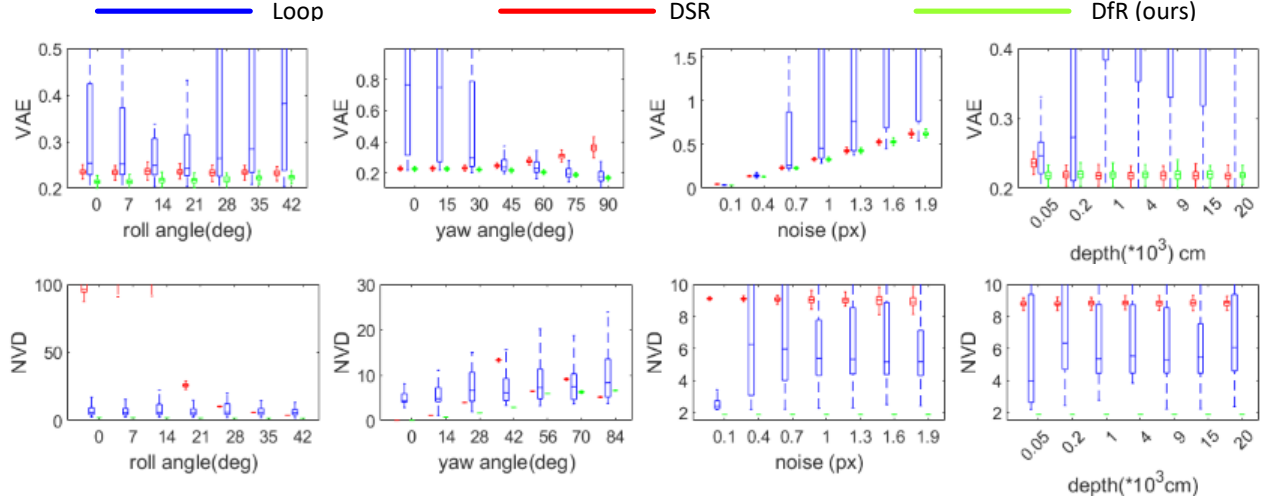


Fig. 6: VAE and NVD scores of the rectification results produced by *Loop*, *DSR* and *DfR* under different settings.

Algorithm 1 DfR (Depth from Rotation)

Input: Uncalibrated stereo images

- 1: Matching correspondences: $\mathbf{p}_i^1 \leftrightarrow \mathbf{p}_i^2, i = 1..N$
- 2: Initialize the vertical direction error: $VER_{min} = \text{inf}$
- 3: **for** $t = 1$ to T **do**
- 4: Randomly select point matches and compute temporary $\hat{\mathbf{H}}_y^1$ and $\hat{\mathbf{H}}_y^2$ using proposition 2 and Eq. (19).
- 5: Calculate VAE by applying $\hat{\mathbf{H}}_y^1$ and $\hat{\mathbf{H}}_y^2$ and take $VAE_{min} = \min(VER_{min}, VAE)$.
- 6: **if** $VAE < VAE_{min}$ **then**
- 7: $VAE_{min} = VAE, \mathbf{H}_y^1 = \hat{\mathbf{H}}_y^1, \mathbf{H}_y^2 = \hat{\mathbf{H}}_y^2$
- 8: **end if**
- 9: **end for**
- 10: Calculate \mathbf{H}_s^1 and \mathbf{H}_s^2 based on Sec. III-B.

Output: $\mathbf{H}^1 = \mathbf{H}_s^1 \mathbf{H}_y^1$ and $\mathbf{H}^2 = \mathbf{H}_s^2 \mathbf{H}_y^2$

◦ *NVD*: We measure the geometric distortion by a normalized vertex distance. Let $\mathbf{v}_1 = [0 \ 0 \ 1]$, $\mathbf{v}_2 = [W - 1 \ 0 \ 1]$, $\mathbf{v}_3 = [0 \ H - 1 \ 1]$, $\mathbf{v}_4 = [W - 1 \ H - 1 \ 1]$ be the four vertices. Then

$$NVD = \frac{d_1 + d_2 + d_3 + d_4}{\sqrt{W^2 + H^2}} \quad (21)$$

where d_i is the distance from \mathbf{v}_i to its rectified point.

• **Setting.** We generated two uncalibrated pin-hole cameras filming a cube scene under latitudinal motion. We set the radius as 1cm and varied the scene depth from 0.5m to 200m, the roll angle between two views from 0 to 45 degs, and the pitch angle from 0 to 90 degs. The results are obtained after averaging the errors over 50 trials at each setting.

• **Results.** The results in Fig. 6 show that the classical rectification method *Loop* [4] provides the most unstable estimation and huge error in VAE. While *DSR* achieves much more robust results and higher accuracy. However, the proposed method *DfR* outperforms *Loop* and *DSR* with a significant

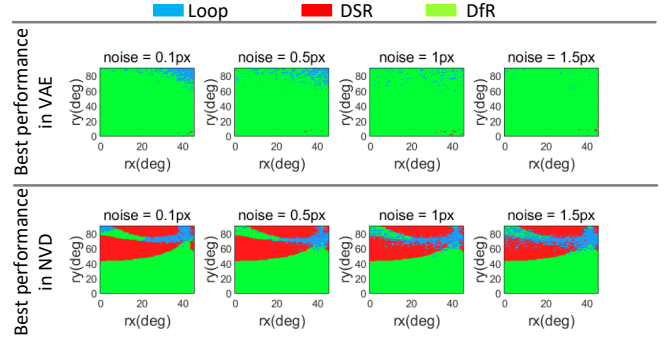


Fig. 7: Best performance among *Loop*, *DSR* and *DfR* in terms of VAE and NVD under different relative poses.

margin. Similarly, *DfR* produces rectified results with much smaller and more stable NVD score than *DSR* and *Loop*, which indicates that the proposed method leads to less geometric distortion. Fig. 7 is to explore in more detail the effect of different conditions on the image rectification results. We mainly modify 3 conditions: the pitch angle ry of the rotating camera swinging left and right, the roll angle rx of the camera swinging up and down, and the image noise. For any points in Fig. 7, the three conditions notes on the vertical axis, the horizontal axis, and the subheadings are shown. Under those conditions, the point is colored green if our proposed method is superior, blue if the method of *Loop* [4] is superior, and red if the *DSR* [6] is superior. *DfR* achieves the best performance in both VAE and NVD under various stereo relative pose settings (roll and pitch).

• **Ablation Study.** We ablate the geometric distortion suppression strategy (Sec. III-B3) used in the proposed *DfR*. As shown in Fig. 5, Visually, *DfR* produces significantly limited distortion over *Loop* and *DSR*. Quantitatively, *Loop* provides the biggest NDV while *DfR* achieves the smallest ones. It is

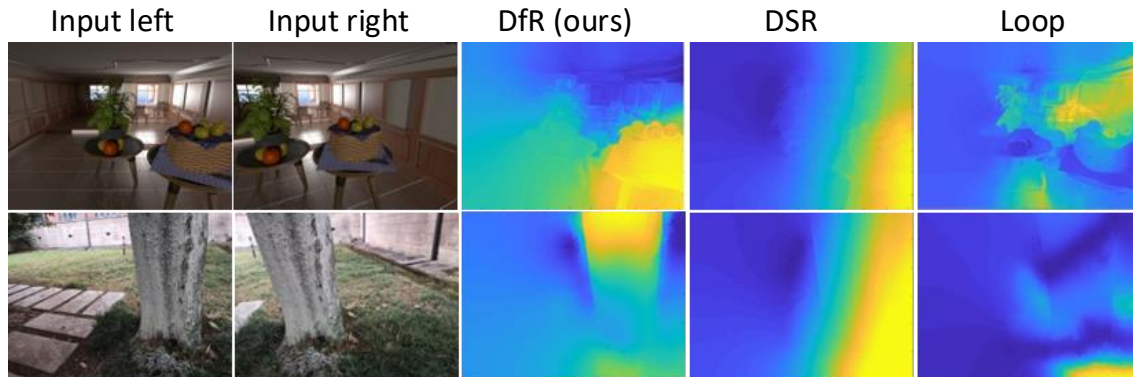


Fig. 8: Comparisons of the depth maps recovered by *Loop*, *DSR* and *DfR*.

Methods	homographies estimation
Loop [4]	14.638 ms
DSR [6]	0.135 ms
DfR(Ours)	0.038 ms

TABLE I: Running time of *Loop* [4], *DSR* [6] and *DfR*.

vital to notice that the geometric distortion becomes larger when we remove the proposed suppression strategy.

• **Running Time.** The experiment was run on a laptop with Intel I5 CPU. the running times are reported in Tab. I with 720×960 pix as input. The results show that *DfR* achieves $4 \times$ and $400 \times$ speedup over *DSR* and *Loop*, respectively.

B. Real Data

To validate the effectiveness of realistic images, we use rotating surveillance cameras to collect 300 pairs of images in various scenarios. We use SIFT feature for detection and matching, followed by stereo rectification with *Loop*, *DSR*, and *DfR*, respectively. Then we perform an SGM dense matching based on the three rectified results to extract the depth images. Results in Fig. 8 show that *Loop* and *DSR* produce blurred depth maps while the proposed approach *DfR* outputs clean and sharp ones instead. This verifies the effectiveness of *DfR* in aligning the point matches into the same row.

V. CONCLUSION

This paper presents a novel image rectification solution to uncalibrated cameras with latitudinal motion assumption. The proposed *DfR* achieves high accuracy in alignment with minor geometric distortion. Extensive experiments demonstrate the effectiveness and efficiency of the proposed solution. The presented *DfR* can be applied as a pre-processing step to stereo matching for many applications, such as 3D visual surveillance and 3D perception of robotics.

REFERENCES

[1] Richard Hartley and Andrew Zisserman, Multiple view geometry in computer vision, 2003.

[2] Andrea Fusiello, Emanuele Trucco, and Alessandro Verri, “A compact algorithm for rectification of stereo pairs,” Machine vision and applications, 2000.

[3] Jonathan Ventura, “Structure from motion on a sphere,” in ECCV, 2016.

[4] Charles Loop and Zhengyou Zhang, “Computing rectifying homographies for stereo vision,” in CVPR, 1999.

[5] Chris Sweeney, Aleksander Holynski, Brian Curless, and Steve M Seitz, “Structure from motion for panorama-style videos,” arXiv, 2019.

[6] Ruichao Xiao, Wenxiu Sun, Jiahao Pang, Qiong Yan, and Jimmy Ren, “Dsr: Direct self-rectification for uncalibrated dual-lens cameras,” in 3DV, 2018.

[7] Zhengyou Zhang, “Determining the epipolar geometry and its uncertainty: A review,” IJCV, 1998.

[8] Joshua Gluckman and Shree K Nayar, “Rectifying transformations that minimize resampling effects,” in CVPR, 2001.

[9] Francesco Isgro and Emanuele Trucco, “Projective rectification without epipolar geometry,” in CVPR, 1999.

[10] Andrea Fusiello and Luca Irsara, “Quasi-euclidean epipolar rectification of uncalibrated images,” Machine Vision and Applications, 2011.